Candel Bou, JJ.; Jiménez, J.; Franconetti Rodríguez, P.; Amigó Borrás, V. (2014). Effect of laser irradiation on failure mechanism of TiCp reinforcedtitanium composite coating produced by laser cladding. Journal of Materials Processing Technology. 214(11):2325-2332. doi:10.1016/j.jmatprotec.2014.04.035.

Effect of laser irradiation on failure mechanism of TiC_p reinforced titanium composite coating produced by laser cladding.

J. J. Candel[1*], J. A. Jimenez[2], P. Franconetti[1], V. Amigó[1]

[1] Universitat Politécnica de Valencia, c\ vera sn, 46022, Valencia (Spain). e-mail: juacanbo@upv.es , Tel: +34963870000 (ext 78451).

[2] Centro Nacional Investigaciones Metalúrgicas (CENIM-CSIC).

Abstract

Laser cladding is an effective technique to coat a metallic substrate with a layer of a different nature. It has been widely reported that the most important combined parameters controlling the quality of the coating are the specific energy (E) and the powder density (Ψ). In the present work, clad deposits of Ti6Al4V+60%wt TiC were prepared on a Ti6Al4V substrate using an optimum combination of E_c = 24 J/mm^2 and ψ_c = 3 mg/mm^2. These experiments were performed using a laser power of 400 and 600 W, in order to study the effect of laser power on the properties of the clad. The microstructure, phase composition and nanohardness of the coatings were investigated by optical microscope, scanning electron microscopy and X-ray diffraction. During laser processing, TiC can be partially converted to TiC_X (X = 0.5) due mainly to the TiC dissolution into the laser-generated melting pool and subsequent precipitation during cooling. It was observed that the lower laser power limit reduces primary TiC dissolution but it also promotes secondary carbide alignment at the interface. On the other hand, the damage mechanism induced by high laser power is dominated by primary TiC particle cracking by the high stress concentration at the particle-matrix interface followed by ductile failure of the matrix. It is also remarkable that irradiance affects the TiC/TiC_x ratio despite E_c and ψ_c are fixed and it determines hardness distribution inside the coating.

Keywords: Coaxial laser cladding, Titanium based composite coatings, Titanium carbide, coating failure mechanism.

Introduction

In our previous review it was analysed the effect of new laser technologies and new coating materials as tools for improving titanium poor wear resistance. It was concluded among the possible materials used as coating it is worth pointing out ceramic particle-reinforced metal matrix composite materials (MMC), especially with Tungsten Carbide (WC) or Titanium Carbide (TiC), due to their excellent combination of hardness and toughness (Candel and Amigo, 2011). But TiC reinforcement can be much more appropriate than WC because of its greater oxidation and corrosion resistance and that why Ti-TiC cermets have being investigated by many authors, for instance Fouilland-Paille et al., (1996) during the last twenty years. As metal matrix there are two main options: the use of Nickel alloys or Titanium alloys. Sun et al., (2002) confirmed that Ni-Cr properties are excellent for the stability of TiC based MMC laser processing, but the use of titanium as metal matrix combined with functionally graded TiC volumetric fraction may involve an interface improve due to mismatch stress reduction with the substrate, as demonstrate Liu and Dupont (2003), and this is a very attractive way to enhance the fatigue life service of laser repaired components.

Zhang et al (2008) confirmed that laser cladding (LC), inside a glove box, is an appropriate technique to apply Ti-MMC selective coatings to complicated shape titanium components. In fact, laser cladding using the powder blowing technique started at the 90s and since then there have been numerous applications in various industrial sectors that made it a promising technique for the future. Of all the possible laser system configurations, the coaxial laser cladding (LC) stands out for its accuracy, versatility, efficiency and quality. And these characteristics have allowed the development of more advanced techniques such as Laser Engineering Near Shape (LENS). Wu and Mei (2003) found that some titanium alloys microstructure is very sensitive to laser parameters, thus LENS process control helps to generate excellent 3D shape components. This path have been followed by several researchers until today and recent works, like Obielodan and Stucker (2013), show LENS deposition of Ti6Al4V/TiC

composites (with TiC contents between 5%wt and 10 wt.%) is able to generate complicated shape components. However it is not a closed research field because the cracking of coatings with high carbide content has not yet been fully elucidated and authors think this must be improved to transfer this knowledge to industry.

At this point, it is important to remind that to obtain Ti-MMC coatings by LC there are two alternative ways: generate TiC in-situ by reaction of elemental powders or using premixed primary TiC particles with titanium and try to reduce to the minimum the dissolution. The first method allows obtaining homogeneous coatings without cracks or pores, an excellent metallurgical bonding but on the contrary the final hardness reached seems to be limited to values lower than 10GPa (Man et al., 2001). When extra hardness is needed, in severe wear applications the second seems to be a better option because it retains primary TiC particles whose hardness can reach 30 GPa. However, this is not a closed research field because avoiding the formation of cracks and obtaining a homogeneous coating is a complex task (Liu et al., 2009).

In the case of high ceramic content Ti-MMC, the optimization of LC processing conditions of titanium alloys is vital. Titanium has a high chemical reactivity with the atmosphere, an elevated melting point and low thermal conductivity. It will therefore be necessary to determine the basic laser parameters of the process (Laser Power, Scanning Speed and Powder Feeding) for working inside a stable process window without oxidation as well as improving the process efficiency. The methodology for this optimization has been developed by many authors, but it is noteworthy the work of Oliveira et al. (2005) on Ni-Cr coatings and Zhou et al. (2009) that analyses the effect of reinforcing with WC in NiCr-WC composites because they established a practical methodology to determine the processing window. Subsequently Fallah et al. (2010) develop this methodology to oxidation sensitive materials like titanium coatings and Emamiam et al. (2011) explained how laser parameters affect the morphology of TiC carbides during Ti-TiC MMC processing by LC.

In our previous work published in 2010 the above methodology was followed. Different Ti6Al4V+X%TiC coatings on Ti6Al4V by coaxial laser cladding were applied and the effect of processing parameters by LC as well as the amount of TiC to increase the dry wear resistance were investigated. Minimizing the dissolution of primary TiC, the wear rate of the MMC coating is ten times lower than the Ti6Al4V substrate (Candel et al., 2010). However, after the industrial application of these coatings some problems of cracking after machining have been found, and this requires further study. Starting from the processing window previously developed for Ti6Al4V layer reinforced with 60%wt TiC, metallurgical transformations associated with cracking phenomena have been studied in this work and are related to laser processing parameters variation inside the optimized processing window.

Experimental set up

2.1Materials and laser equipment

Two different powders were used as coating: spherical argon atomized Ti6Al4V powder (99.5% purity) with a 35<D<75μm particle size and another irregular TiC powder (99.9% purity and 20%wt minimum carbon content guaranteed) that was sieved between 38<D<50μm. Both powders were supplied by TLS Technik and AEE respectively and they were mixed before laser processing using a tumbler mixer inside an argon sealed container in order to obtain an homogenous mixture of Ti6Al4V+60%TiC in mass with an optimum powder fluidity. The objective of TiC sieving is the reduction of particle size variability with a double purpose: i) to enhance powder flowing rate; ii) to facilitate TiC dissolution analysis after laser processing. As substrate a Ti6Al4V plate of 5mm in height was used. The surface was grinded using P500 silicon carbide paper and it was degreased with acetone previously to laser irradiation.

It has been used an industrial cladding system composed by a solid-state Nd:YAG laser operated in continuous mode with maximum power of 2kW, equipped with coaxial cladding nozzle and powder feeder. The diameter of the laser beam spot size on the workpiece's surface was fixed at 2 mm. The laser machine is integrated in a 6 axis industrial robot that allows

depositing coatings in the workpiece with a 0.05mm precision. To protect the melt pool from oxidation, Helium shielding gas was supplied through cladding head at 20 $l \cdot min^{-1}$.

2.2Experimental design

The laser processing parameters

All the processing parameters (laser power, scanning speed, beam diameter, powder feeding, shielding gas...) affect the quality of the clad, but not independently. For this reason, it is important to define combined process parameters to simplify the optimization process as mentioned by Oliveira et al. (2005) and Fallah et al. (2010).

There are two basic combined parameters, developed by the authors mentioned above, to study the processing of titanium by LC: laser specific energy (E) and powder density (ψ). The use of these parameters can reduce the experimentation in the laboratory and the processing window can be easily transferred to other industrial equipment with minor modifications.

Both parameters can be defined as:

$$E = \frac{P}{V \cdot D} \quad (1)$$

$$\psi = \frac{F}{V \cdot D} \quad (2)$$

Where P is the laser power (W), V is the scanning speed (mm/s), F is the powder feed rate (g/s) and D is the beam diameter (mm).

Fallah et al. (2010) propose that the LC optimization process consists of adjusting each of these two parameters to achieve an acceptable quality clad. Using this approach, the advantage is that both parameters are proportional, that is, for each value of ψ there is a critical value of E below which the quality is not acceptable.

In our previous work (Candel et al., 2010) this methodology was followed in our laboratory and it was found that to maximize the dry wear resistance the combination of parameters most appropriate for Ti6Al4V +60% TiC was E_c = 22J/mm^2 and ψ_c = 3 mg/mm^2. Now this processing window has been transferred to other industrial laser system and it has been slightly modified to fit this new equipment. However, although the coatings had no defects after visual inspection, the industrial process of machining and polishing revealed significant differences when changing the laser irradiance, although E_c and ψ_c stay constant. Effect of laser irradiance during LC processing of Ti-MMC coatings was first reported by Emamiam et al. (2011) study about the generation "in situ" TiC particles. But authors have detected that the coaxial LC process using high volume of TiC powder particles is very sensitive to small changes in laser irradiance, since it affects the failure mode of the coating. Thus, a further study is required to clarify the relationship between all this variables.

In this work, two different coatings of 15x30mm have been deposited with the parameters shown in Table 1. It would be possible to increase slightly the value of E with the same laser power (e.g. reducing V) to avoid the cracking problem, but previous results suggest this strategy lowers the wear resistance due to the dissolution of primary carbides (Candel et al 2010). The main problem addressed in this paper is to reduce cracking but keeping the amount of primary carbides as high as possible thus E was fixed to 24J/mm^2.

After the laser processing, the surface of both coatings has been machined using a universal grinder machine equipped with a corundum wheel. The industrial process is divided in two steps: material removing and subsequent polishing step in order to obtain a flat surface of the component with an average roughness R_a <1μm.

Materials characterization

The coatings microstructure was characterized using a Nikon LV100 optical microscope, a Hitachi 4800 FESEM equipped with an energy dispersive X-ray spectrometer (EDS), and a Siemens D-5000 diffractometer equipped with X-ray Cu tube and a diffracted beam

monochromator. For the observation of the microstructure, a cross-section of each coating was obtained using a precision table top cut-off machine to minimize the cracking phenomenon. Metallographic specimens were not etched and the polishing procedure included a final ultrapolishing step with 90ml colloidal silica (40 nm) + 10ml H_2O_2 suspension to remove the deformed layer.

Table 1. Selected laser parameters for coatings

Id	P(W)	V(mm/s)	F(g/s)	E(J/mm^2)	Ψ(mg/mm^2)
Coating 1	400	8.3	0.050	24.0	3.0
Coating 2	600	12.5	0.075	24.0	3.0

In order to estimate the chemical composition of each phase, EDS semi-quantitative analyses were performed. These results have been just used for qualitative purpose, to determine differences between phases present in the microstructure, due to two inherent limitations of the technique: i) the small size of the carbides in some cases and the microprobe measuring affected area by a point analysis that include large part of matrix around them; ii) the low accuracy of carbon measurement by EDS.

Identification of the crystalline phases in the coating was conducted by X-ray diffraction (XRD). XRD- measurements were carried out at a current of 30 mA and a voltage of 40 kV as tube setting. Operational conditions were selected to obtain X-ray diffraction diagrams of sufficient quality: sufficient counting statistics, narrow peaks and detection of small diffraction peaks of minor phases. XRD data were collected over a 2θ range over a 2θ range of 20 -120º with a step width of 0.03º and a counting time of 5 s/step. The phase present in the XRD patterns have been identified using the JCPDS database and the DIFFRACplus EVA software by Bruker AXS.

The most important structural parameters of the XRD profiles were determined by the Rietveld method. We have used the version 4.0 of Rietveld analysis program TOPAS (Bruker AXS) for the XRD data refinement. In this work, instrument functions were empirically parameterized

from the profile shape analysis of a corundum sample measured under the same conditions. The refinement protocol included also the major parameters like, background, zero displacement, the scale factors, the peak breath, the unit cell parameter and texture parameters. The quality and reliability of the Rietveld analysis was quantified by the corresponding figures of merit: the weighted summation of residual of the least squares fit, $R_{wp,}$ the statistically expected least squares fit, R_{exp}, the profile residual, R_p, and the goodness of fit (sometimes referred as chi-squared), GoF (Pecharsky and Zavalij, 2005). Since GoF = R_{wp} / R_{exp}, a GoF = 1.0 means a perfect fitting.

The room temperature structures used in the refinement were α-Ti and the carbide TiC. The α-Ti has a hexagonal close packed (hcp) structure (space group P63/mmc) with two atoms per unit cell at (1/3,2/3,1/2) and (2/3,1/3,3/2). On the other hand, the TiC carbide has a cubic NaCl-type crystal structure (space group *Fm*3*m*) which is described as a cubic-F with a motif consisting of a Ti atom at (0, 0, 0) and a carbon atom at (0, 0, 1/2). But Quinn and Kohlstedt (1984) confirmed that this carbide can exhibit non-stoichiometry over a wide range without the change of crystal structure when it reacts with molten titanium metal, leading to substoichiometric TiC_X with $0.47< x < 1$.

Nanoindentation experiments were performed using MTS G200 Nanoindenter equipped with previously calibrated Berkovich tip. To ensure enough population of tests, the cross-section of each coating was analysed using a 15 x 10 = 150 indents grid with 10 μm spacing. Tests were conducted using Continuous stiffness measurement method (CSM) at 2 nm and 45Hz harmonic oscillation in order to determine the hardness of each present phase. Considering the size of the constituents, the maximum penetration depth was limited to 300 nm and the hardness value was averaged in the stable range of depth between 100 to 200 nm. After nanoindentation, FESEM observation was used to reject atypical tests that present non-desirable features due to surface irregularities (p. e. at the interface between two phases) or an anomalous behaviour due to pile-up, sink-in or cracking superficial effect. These effects are out of the scope of this work.

Results and discussion

The visual inspection of the coating surface after laser processing was the first step for coating characterization. It has been confirmed that general quality criteria for laser cladding, defined by other authors like Zhou et al. (2009) and Fallah et al. (2010), are accomplished:

- Formation of a continuous bead fully adhered to the substrate.
- Formation of clearly observable and straight root edges.
- Absence of visual cracks and pores.
- Silver coloured coatings without other coloured oxides.

Visual inspection of both coatings revealed a good and continuous layer, thanks to closed loop control of the process at the starting and ending point of each single track, without signs of surface cracks, pores or lack of adhesion. As shown in Figure 1, no defects were found on coatings surface, and therefore they were sent to the machining process to achieve the flat and polished surface essential for the desired industrial application.

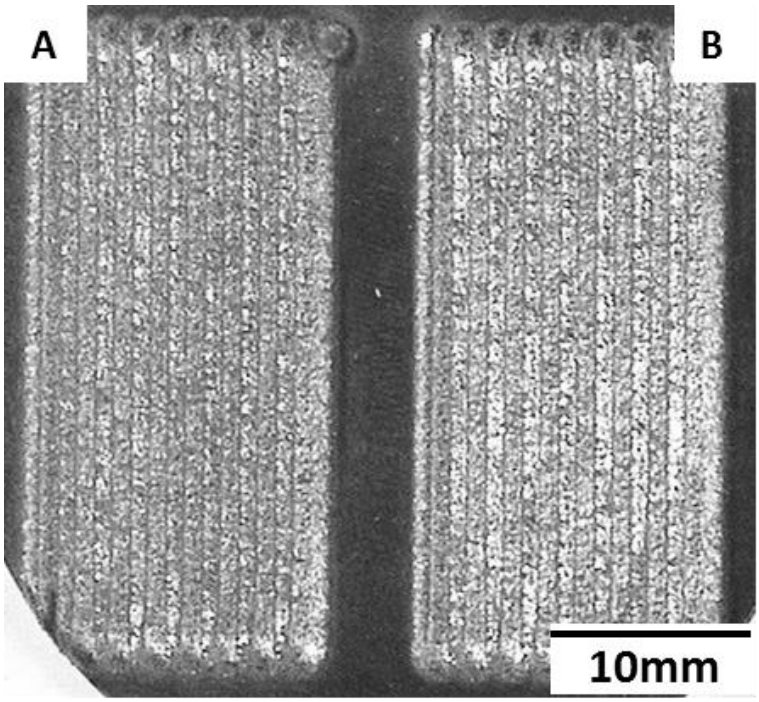

Figure 1. General appearance of laser cladding coatings **before** machining: A) *P*=400W; B) *P*=600W.

After the machining process both coatings present defects, see Figure 2, but the impact of the defects is different in each case. Henceforth further investigation for microstructure determination (chemical composition, phase constitution and morphology) will be discussed for each coating separately. They constitute the lower and upper laser power limit inside the optimized laser processing window (E_c=24J/mm^2; ψ_c=3mg/mm^2) and they present different failure mode. At the end of the work, to sum up the results, it will be compared the hardness distribution of both coatings in order to examine other laser irradiance related effects.

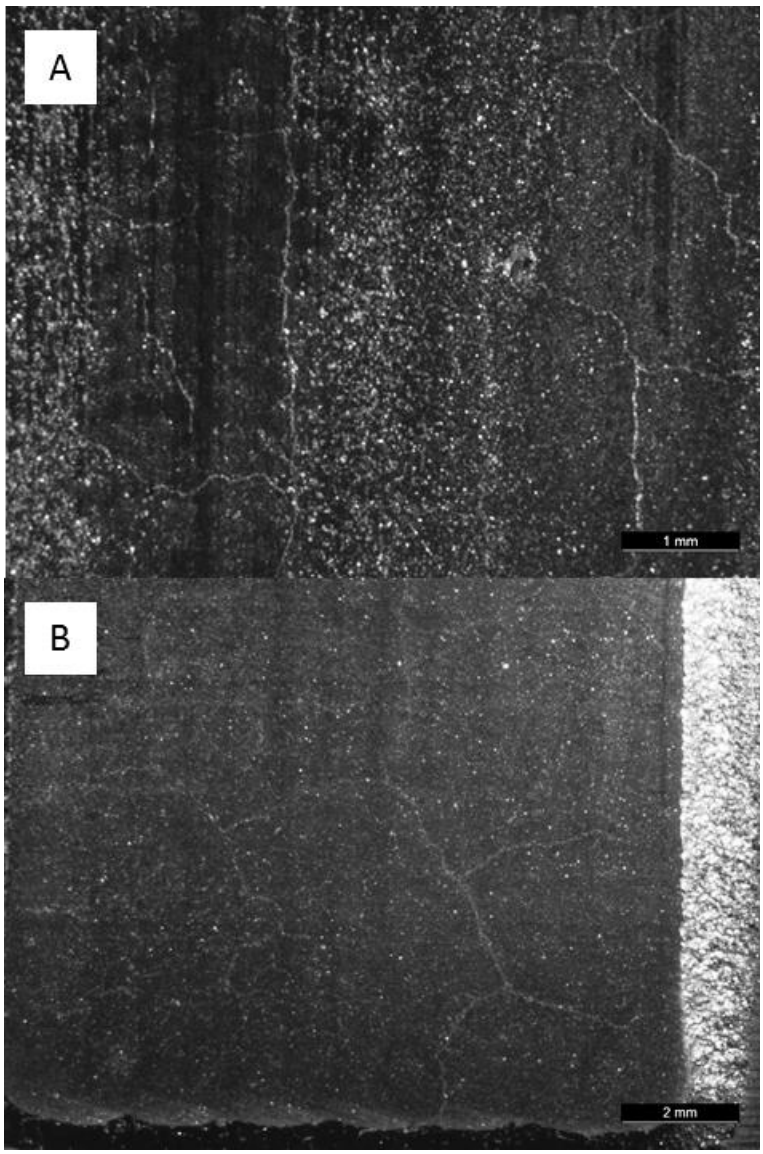

Figure 2. Cracks detected **after** the machining process of the coatings: A) Coating 1, P=400W; B) Coating 2, P=600W.

Analysis of low laser irradiance combined with low scanning speed coating (Coating 1; P*=400 W; V=8.3 mm/s)*

As observed in Figure 2A, machining process has generated numerous cracks in almost all the tracks; they are aligned with the laser scanning direction and transversally interconnected. It was not possible to achieve a polished surface due to its extreme hardness and fragility, thus machining marks are observed.

Before microstructure discussion, it is important to remark that it has been used a powder blend of 60%wt (TiC) + 40%wt (Ti6Al4V). If all primary carbides were dissolved and precipitated it would give an approximate carbon molar fraction of 0.35, then the resulting microstructure should be completely TiC_x. However, during the laser processing there is not enough interaction time to complete carbon diffusion. Hence, there are areas between primary particles where the carbon content can be increased and others far from the carbides with less than 0.35 molar fraction.

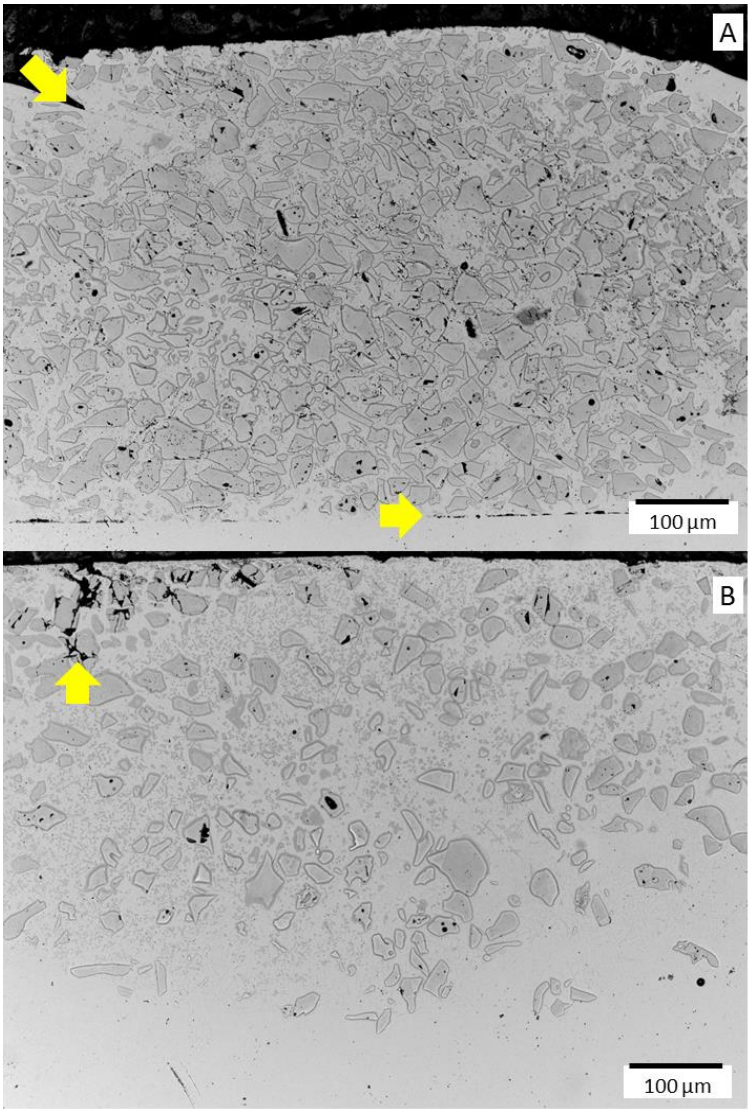

Figure 3. Optical image of laser clad cross-section: A) P= 400 W; B) P=600W. Arrows depict detected micro-cracks after machining.

Laser parameters of Coating 1 represent a lower limit value of laser irradiance inside the processing window marked by E_c = 24J/mm^2; ψ_c = 3mg/mm^2. Figure 3A reveals the presence of irregularly-shaped, uniformly-distributed primary TiC reinforcing particles in the laser clad coating. Some of those particles include inside dark areas, which correspond to voids. But contrary at it should be expected, cracks are nucleated in areas where are not present a high volume fraction of those TiC particles. As indicated in this figure by arrows, cracks propagate at the interfaces coating-substrate and the overlapping of consecutive tracks. These cracks at the coating/substrate interface are nucleated to interconnect the pores due to not complete substrate melting during laser cladding (figure 4)

The primary root cause of the coating cracking is the precipitated ultrafine carbides alignment and the progression of cracks through the interface during the coating cooling or machining process (detail 4A). Only a small amount of primary TiC particles were melted, dissolved and precipitated in titanium matrix (detail 4B). The low irradiance of the Nd:YAG laser in this case and the difference in laser radiation absorption and thermal conductivity between Ti6Al4V and TiC, limits the dissolution of the reinforcing particles.

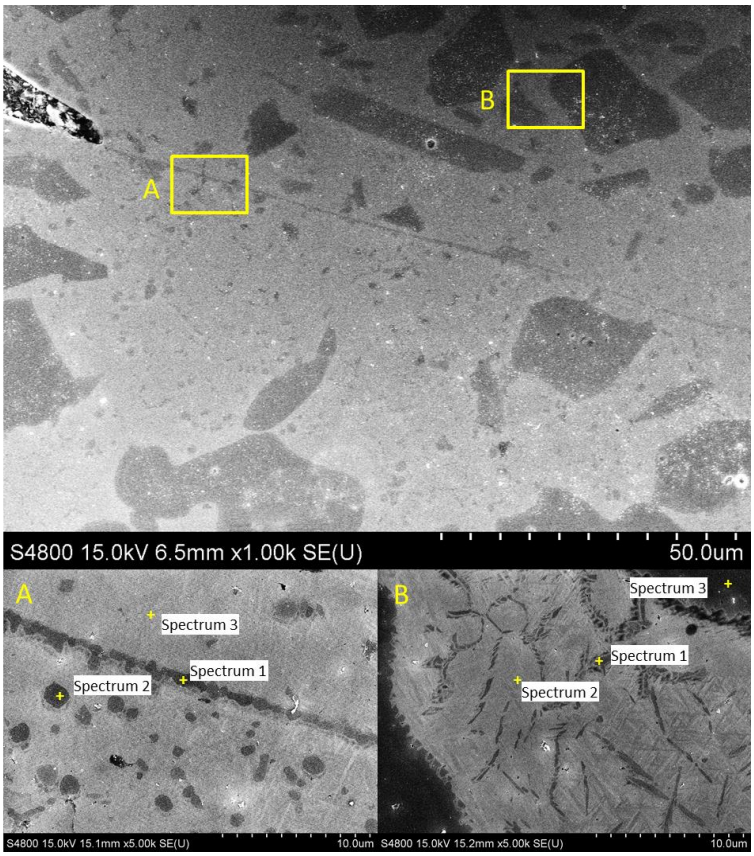

Figure 4. FESEM micrographs showing crack propagation through aligned secondary carbides at the overlapping zone between single tracks of coating 1.

As shown in Figure 5, XRD pattern of the machined surface of coating 1 shows a mix of two phases: α-Ti (JCPDS card 035-0121), and TiC (JCPDS card 046-1212). Although the initial powder blend consist of a powder mixture of TiC and Ti6Al4V, in the coating prepared by laser processing TiC can be partially converted to TiC_X due mainly to the TiC dissolution into the laser-generated melt. However, matching the XRD pattern with the JCPDS database did not allow to unambiguously characterizing TiC and TiC_X carbides due to systematic peak overlap.

This problem can be overcome by using the Rietveld refinement based on a mixed of α-Ti, TiC and TiC_X. The goodness of this analysis was confirmed by a GoF = 1.26. Rietveld refinement has been widely reported as one of the most suitable technique for quantification of crystalline phases in a given material from the X-ray diffraction pattern (Rietveld, 1969). However, the quantitative phase analysis as obtained by the Rietveld refinement overestimated the amount of carbide presents in the coating. Since penetration of Cu Kα radiation in conventional XRD measurements is limited to a few microns of depth, XRD patterns will provide information only of the outer layer of the coating.

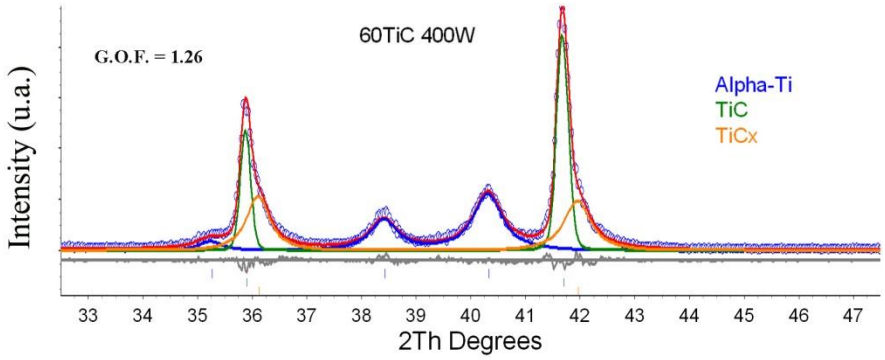

Figure 5. Rietveld refinement of Coating 1 XRD pattern.

Zeng et al. (1996) established the motion mode of ceramic particles inside laser cladding composite coatings demonstrating that it exists an stirred mode in which particles moves along the coating due to not only to physical properties (density mismatch, particle size or melting pool shape, for example) but also due to chemical interaction between molten metal and ceramic particle that modifies the specific energy of the process. Probably this is the cause of a higher amount of un-melted TiC carbides particles at the top of the laser cladding, but the determination of the motion mode is out of scope of the present work.

Although primary TiC particles do not undergo considerable melting/dissolution, X-ray diffraction studies confirmed the presence of non-stoichiometric TiC_X. Examination of the coating at higher magnification using FESEM revealed numerous carbide particles with a size

much smaller than the initial powder, and the presence of a reaction layer at the interface between the TiC particles and the matrix, as shown in Figure 4B. EDS analysis confirms a different chemical composition between primary and secondary TiC carbides, precipitated particles have higher V and a lower C content (see Table 2). As V is a β stabilizer, precipitation of non-stoichiometric TiC_X containing V will decrease the amount of this element on the molten matrix material. For this reason, β−Ti phase was not detected in the XRD spectra, indicating that all the matrix material had been transformed to α-Ti.

Table 2. Summary of the punctual EDS microanalysis of the coating 1 marked in the Figure 4

Figure 4A				
%wt	C	Al	Ti	V
Spect 1	12.58	2.21	83.21	2.00
Spect 2	14.09	2.53	81.24	2.14
Spect 3	4.47	5.61	85.42	4.49
Figure 4B				
Spectrum	C	Al	Ti	V
Spect 1	13.69	3.32	80.21	2.78
Spect 2	4.18	6.27	84.99	4.56
Spect 3	23.43		76.57	

When TiC particles partially dissolve during laser processing, the liquid metal is enriched with carbon. According to the C-Ti phase diagram of Uhrenius (1984), solidification of this carbon rich melt starts with the formation of primary TiC_X particles, until the eutectic temperature is reached. At this temperature, the remaining liquid decomposes to form β−Ti with 0.006C molar fraction (≈ 0.5% wt) and $TiC_{0.5}$ with a molar fraction of 0.32C (≈ 11% wt), and the solidification process is finished. Although almost no change in carbide microstructure will take place during cooling after solidification, β−Ti will transform to α-Ti at the β−transus temperature (≈ 900ºC). Because of the high cooling rate associated to the laser cladding process, this transformation is

expected to occur martensitically. Thus, the coating microstructure at room temperature consists of martensitic α'-Ti in a Widmanstatten pattern.

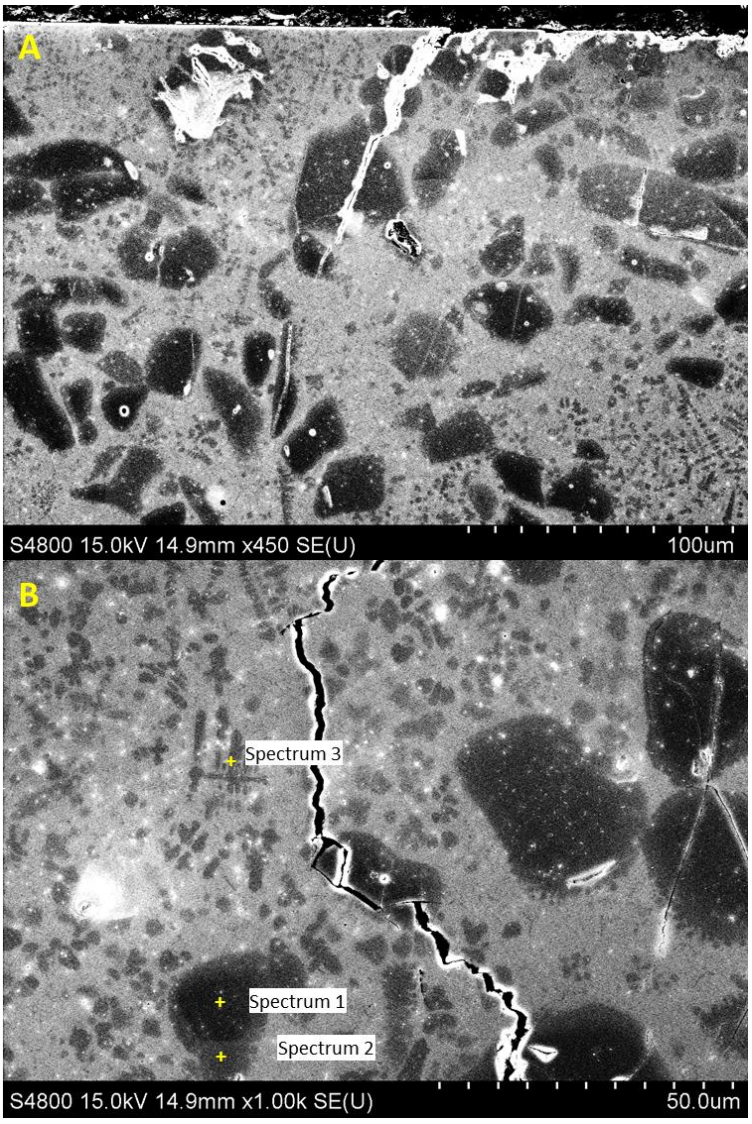

Figure 6. FESEM micrograph showing micro-cracks inside primary TiC carbides located near the coating surface (A) and crack propagation after machining of the coating 2 (B).

Analysis of High laser irradiance combined with high scanning speed coating (Coating 2)

Changing processing conditions induces a different coating failure mechanism. As observed in figure 2B, machining process has generated less cracks and better surface finishing in comparison with coating 1. Micro-cracks were observed mostly inside primary TiC carbides located near the top coating surface, see figure 3B. The formation of this type of cracks is

associated with the thermal stress produced by rapid solidification process during laser cladding. The stress concentration in the interface between the hard TiC particles and the metal matrix arise from the difference in the thermal and physical properties of the two phases in both sides of the interface. The micro-cracks formed inside the TiC particles can be easily propagated during machining from the external flat surface, as shown in Figure 6A. Therefore, coating 2 constitutes the upper limit value of laser irradiance inside the processing window marked by E_c = 24J/mm^2; ψ_c = 3mg/mm^2. If laser power is bigger than 600W failure occurs due to micro-crack nucleation inside the TiC particles by the high stress concentration at the particle-matrix interface. Then, although visual inspection of the coating seems to be correct, the propagation of those cracks through the coating will take place during machining process.

In this case, the higher laser power (600W) combined with a high scanning speed enhances primary TiC particle melting/dissolution. Coating 2 shows a lower volume fraction of primary TiC reinforcing particles in the laser clad than coating 1 (compare figure 3A and 3B). A closer examination of zone around these TiC particles revealed the effects of melting and diffusion around the blocked particles into the matrix, see figure 6B. EDS analysis of these regions around the TiC particles show a lower C content inside primary TiC particles. Furthermore, it has been probed the high diffusion of carbon into the titanium molten matrix during laser processing (see Table 3). Therefore, during cooling, primary dendrites of TiC_X can be precipitated from the liquid phase, followed by a eutectic reaction, as explained before. FESEM micrograph at higher magnification of the matrix surrounding the primary TiC shows the presence of a dark-contrast dispersed phase with a dominant dendritic morphology, as in Figure 6B.

Table 3. Summary of the punctual EDS microanalysis of the coating 2 marked in the Figure 6

%wt	C	Al	Ti	V
Spect 1	17.27		82.73	
Spect 2	16.02	0.86	81.37	0.76
Spect 3	11.92	0.94	85.50	1.63

The results of the X-ray diffraction test revealed a pattern very similar to that of Figure 5. As shown in figure 7, the Rietveld refinement confirms the presence of α-Ti, TiC and TiC_X. Although XRD provides only information of the outer layer of the coating, the relative diffraction intensity between the TiC and TiC_x decreases, which means that the fraction of primary TiC decreases. However, the overall carbon content and the lattice parameter value (0.4300 ± 0.0002 nm) for these carbides are similar in both coatings.

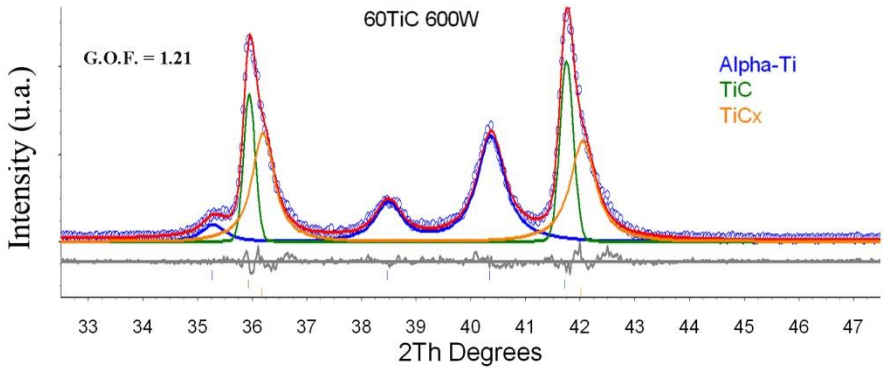

Figure 7. Rietveld refinement of the coating 2 XRD pattern.

Analysis of the effect of laser irradiance on hardness distribution

Typical curves of hardness evolution using CSM method and FESEM micrographs of the residual indentation after 500nm penetration depth are shown in Figure 8. Penetration depth for hardness (H) calculation was limited to 100-200 nm range in order to avoid undesirable superficial effects as well as the roundness of the indenter tip. The goodness of the calculation method can be observed in the H constant value inside this range for α-Ti matrix and primary TiC particles in the Figure 8. Caceres et al. (2008) have reported that alfa titanium nanohardness is around 4 GPa, but the eutectic transforms the liquid in a fine dispersion of $Ti+TiC_x$ (X=0.5), thus hardening of the matrix is expected. It has been confirmed that this reaction produces a slight increase in hardness till 4<H<7GPa as can be seen at figure 8B.

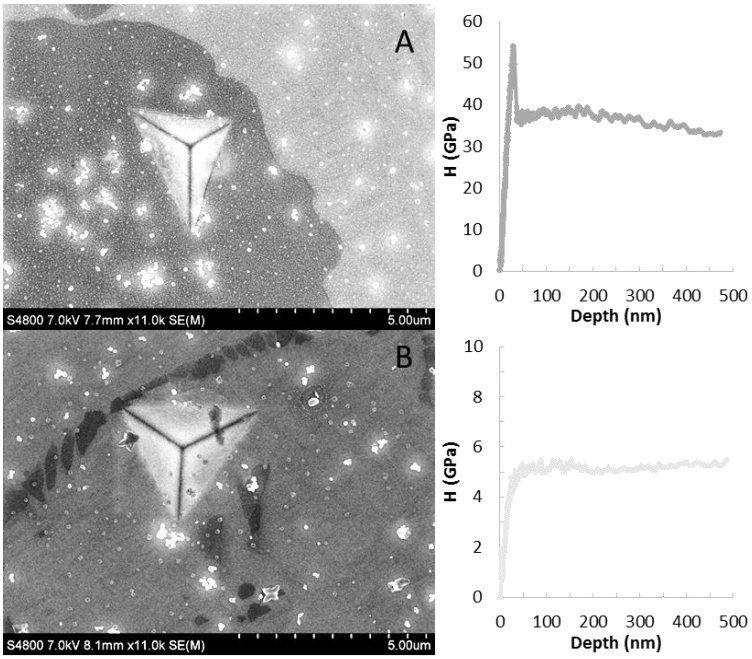

Figure 8. FESEM micrograph and CSM Hardness curve obtained by nanoindentation tests inside primary TiC particle (a) and eutectic α-Ti+TiCx matrix (B).

But the most interesting was the effect of the TiC dissolution on carbide nanohardness. Mani et al. (2005) have reported TiC nanohardness, during sputtering deposition process, depends on carbon content but this behaviour cannot be directly extrapolated to a laser process that has a laser-particle time interaction as low as 0.2s. It has been found a marked difference between measurements in the core of primary TiC particles (H>30GPa, see figure 8A) and the ones that were measured in the reaction layer of primary TiC or inside rounded-shape carbides that have been partially dissolved.

Effects of laser irradiance can be summarized in the hardness distribution of each coating using a frequency histogram, see Figure 9. Coating 1, processed with low laser power (P = 400W), shows a bimodal distribution of primary carbides hardness 30-40GPa inside titanium matrix (H <4GPa) slightly hardened by the presence of the eutectic Ti+TiC_x (4 <H <7GPa). Laser power increasing in the coating 2 (P = 600W) reduces the fraction of primary carbides but increases the amount of carbon content in the liquid formed. Therefore, the amount of secondary carbides nucleated in the form of spherical particles or dendrites is bigger and the presence of the eutectic

inside the matrix will be more important. The verification of this hypothesis can be supported by the almost continuous distribution between 7GPa and 30GPa as well as the augment of eutectic column in the coating 2.

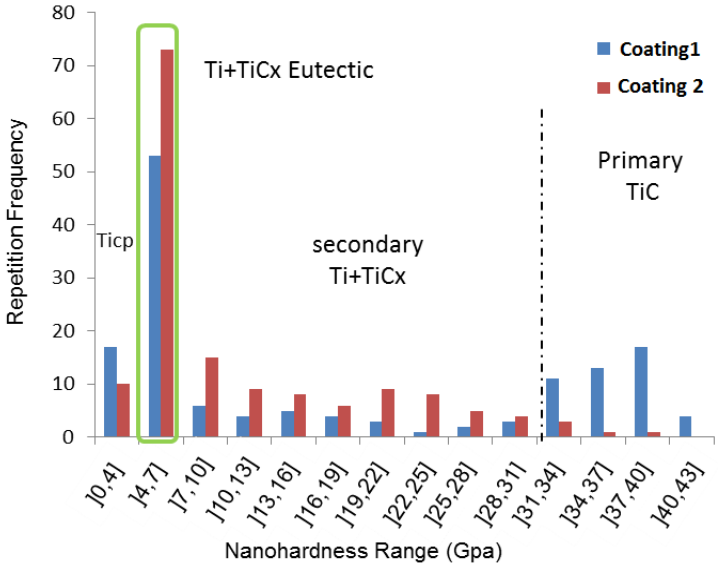

Figure 9. Hardness distribution after nanoindentation tests in the cross-section of the coatings.

Conclusions

a) Laser cladding of Ti6Al4V+60 wt. %TiC inside the processing window defined by E_c = 24 J/mm^2 and ψ_c = 3 mg/mm^2 gave a uniform clad with the two levels of laser power used, 400 and 600W. In both cases, it was found that TiC particles partially or wholly dissolved in the Ti alloy promote the precipitation of dendrites of TiC_X during cooling from the liquid phase. The amount of dissolved carbide increases with the power of the laser beam. However, the carbon content in the TiC_X is similar in both coatings.

b) It was observed a change in the coating failure mechanism by increasing the power used for processing. At low laser power limit, the failure was due to interfacial cracking and cracks propagation at the interfaces coating-substrate and the overlapping of consecutive tracks. At higher laser power, the failure can occur due to microcrack nucleation at the TiC particles by the high stress concentration at the particle-matrix interface, and propagation of those cracks through the coating.

c) Nanoindentation tests show that low laser power level produces a bimodal hardness distribution typical of composite materials, composed by α-Ti metallic matrix (H<4GPa) and TiC primary particles (H>30GPa). An augment of laser irradiance reduces maximum hardness due to primary TiC dissolution but it produces a continuous distribution between both categories due to secondary carbide precipitation.

d) Carbon diffusion produces a continuous nanohardness distribution between 30GPa and 7GPa. Therefore it is not only important retain primary TiC particles but also augment its carbon content. Authors think that an addition of graphite to the powder blend could be an interesting way for futures works in order to improve the results.

Acknowledgments

Authors thank MINECO funding in special the Training of Research Staff program with the help BES-2009-013589 and the support of the Comisión Interministerial de Ciencia y Tecnología (CICYT), Spain, under Grant MAT2012-39124. This work was developed at the Materials Technology Unit of the Polytechnic University of Valencia associated to CSIC through the National Centre for Metallurgical Research (CENIM). Finally, thank the EU for the funding received through the FEDER help in the project UPOV08-3E-005 for the purchase of equipment and the Generalitat Valenciana for the help ACOMP/2012/094.

References

Caceres, D., Munuera, C., Ocal, C., Jiménez, J.A., Gutiérrez A., 2008. Nanomechanical properties of surface-modified titanium alloys for biomedical applications. Acta Biomater. 4, 1545–1552.

Candel, J. J., Amigó, V., 2011. Recent advances in laser surface treatment of titanium alloys. J. Laser Appl. 23, 1-7.

Candel, J.J., Amigó, V., Ramos, J.A., Busquets, D., 2010. Sliding wear resistance of TiC_p reinforced titanium composite coating produced by laser cladding. Surf. Coat. Tech. 204, 3161-3166.

Emamian, A., S. Corbin, S. F., Khajepour, A., 2011. The influence of combined laser parameters on in-situ formed TiC morphology during laser cladding. Surf. Coat. Tech. 206,124-131.

Fallah, V., Corbin, S.F., Khajepour A., 2010. Process optimization of Ti–Nb alloy coatings on a Ti–6Al–4V plate using a fiber laser and blended elemental powders. J. Mat. Proc. Tech. 210, 2081–2087

Fouilland-Paille, L., Ettaqi, S., Benayoun, S., Hantzpergue, J.J., 1996. Structural and mechanical characterization of Ti/TiC cermet coatings synthesized by laser melting. Surf. Coat. Tech. 88, 204-211.

Liu, L., Zhang, S.Q., Li, A., Wang, H.M., 2009. Microstructure and tensile properties of laser melting deposited TiC/TA15 titanium matrix composites. J. Alloys Comp. 485, 156–162.

Liu, W., DuPont, J.N., 2003. Fabrication of functionally graded TiC/Ti composites by Laser Engineered Net Shaping. Scripta Mater. 48, 1337–1342.

Man, H. C., Zhang, S., Cheng, F. T., Yue, T. M., 2001. Microstructure and formation mechanism of in situ synthesized TiC/Ti surface MMC on Ti-6Al-4V by laser cladding. Scripta mater. 44, 2801–2807.

Mani, A., Aubert, P., Mercier, F., Khodj, H., Berthierd, C., Houdy, P., 2005. Effects of residual stress on the mechanical and structural properties of TiC thin films grown by RF sputtering. Surf Coat Tech. 194, 190– 195.

Obielodan, J., Stucker, B., 2013. Characterization of LENS-fabricated Ti6Al4V and Ti6Al4V/TiC dual-material transition joints. Int J Adv Manuf Technol. 66, 2053–2061.

Oliveira, U., Ocelik, V., De Hosson, J.Th.M., 2005. Analysis of coaxial laser cladding processing conditions. Surf. Coat. Tech. 197, 127–136.

Pecharsky, V. K., Zavalij, P. Y., 2009. Fundamentals of powder diffraction and structural characterization of materials, second ed. Springer, New York, pp. 407-495.

Quinn C. J., Kohlstedt, D.L., 1984. Solid-State Reaction Between Titanium Carbide and Titanium Metal. J. Amer. Ceram. Soc. 67:305-310

Rietveld, H. M., 1969. A profile refinement method for nuclear and magnetic structures. J. Appl. Crystallogr. 2, 65-71.

Sun, R. L., Mao, J. F., Yang, D. Z., 2002. Microscopic morphology and distribution of TiC phase in laser clad NiCrBSiC–TiC layer on titanium alloy substrate. Surf. Coat. Tech. 155, 203–207.

Uhrenius B., 1984. Calculation of the Ti-C, W-C and Ti-W-C phase diagrams. Calphad. 2,101-119

Wu, X., Mei, J., 2003. Near net shape manufacturing of components using direct laser fabrication technology. J. Mater. Process. Tech. 135, 266–270.

Zeng, X., Tao, Z., Zhu, B., Zhou, E., 1996. Investigation of laser cladding ceramic-metal composite coatings: processing modes and mechanisms. Surf. Coat. Tech. 79, 209-217.

Zhang, Y., Wei, Z., Shi, L., Xi, M., 2008. Characterization of laser powder deposited Ti–TiC composites and functional gradient materials. J. Mater Process. Tech. 206, 438-444.

Zhou, S., Dai, X., Zeng, X., 2009. Effects of processing parameters on structure of Ni-based WC composite coatings during laser induction hybrid rapid cladding. Appl. Surf. Sci. 255, 8494–8500.